crystals

MDPI

Article

Effect of Rare-Earth Element Oxides on Diamond Crystallization in Mg-Based Systems

Yuri N. Palyanov [1,2,*], Yuri M. Borzdov [1], Alexander F. Khokhryakov [1,2] and Igor N. Kupriyanov [1]

[1] Sobolev Institute of Geology and Mineralogy SB RAS, Koptyug ave. 3, 630090 Novosibirsk, Russia; borzdov@igm.nsc.ru (Y.M.B.); khokhr@igm.nsc.ru (A.F.K.); spectra@igm.nsc.ru (I.N.K.)

[2] Department of Geology and Geophysics, Novosibirsk State University, 630090 Novosibirsk, Russia

* Correspondence: palyanov@igm.nsc.ru; Tel.: +7-383-330-7501

Received: 14 May 2019; Accepted: 10 June 2019; Published: 11 June 2019

Abstract: Diamond crystallization in Mg-R_2O_3-C systems (R = Nd, Sm, Eu, Tb, Dy, Ho, Er, Tm, and Yb) was studied at 7.8 GPa and 1800 °C. It was found that rare-earth oxide additives in an amount of 10 wt % did not significantly affect both the degree of graphite-to-diamond conversion and crystal morphology relative to the Mg-C system. The effect of higher amounts of rare-earth oxide additives on diamond crystallization was studied for a Mg-Sm_2O_3-C system with a Sm_2O_3 content varied from 0 to 50 wt %. It was established that with an increase in the Sm_2O_3 content in the growth system, the degree of graphite-to-diamond conversion decreased from 80% at 10% Sm_2O_3 to 0% at 40% Sm_2O_3. At high Sm_2O_3 contents (40 and 50 wt %), instead of diamond, mass crystallization of metastable graphite was established. The observed changes in the degree of the graphite-to-diamond conversion, the changeover of diamond crystallization to the crystallization of metastable graphite, and the changes in diamond crystal morphology with increasing the Sm_2O_3 content attested the inhibiting effect of rare-earth oxides on diamond crystallization processes in the Mg-Sm-O-C system. The crystallized diamonds were studied by a suite of optical spectroscopy techniques, and the major characteristics of their defect and impurity structures were revealed. For diamond crystals produced with 10 wt % and 20 wt % Sm_2O_3 additives, a specific photoluminescence signal comprising four groups of lines centered at approximately 580, 620, 670, and 725 nm was detected, which was tentatively assigned to emission characteristic of Sm^{3+} ions.

Keywords: diamond; high-pressure; high-temperature; crystallization; crystal morphology; rare-earth ions; defects; characterization

1. Introduction

The combination of unique properties of diamonds predefines the potentials for its application in various fields of science and technology, including a new direction related to quantum technologies. Particular attention has been drawn to diamond as a perfect host for various optically active defects, the most important of which is the nitrogen-vacancy (N-V) center. The remarkable optical and spin properties of N-V centers have boosted extensive research on diamonds targeting novel quantum applications, including solid-state single photon sources [1,2], nanoscale electromagnetic field sensing [3,4], biolabeling [5,6], quantum optics [7], and quantum information processing [8,9]. Recently, color centers caused by group-IV elements with vacancies—Si-V, Ge-V, Sn-V, and Pb-V [10–17]—have received a lot of attention because of their outstanding spectral properties. In recent years, in the search for new color centers promising for quantum technology applications, there has been growing interest in producing diamonds doped with rare-earth (RE) elements. It is well known that rare-earth ions have unique optical and magnetic properties and are widely used in various areas of modern technologies, including solid-state light sources, imaging, and telecommunication systems. Particularly noteworthy are their narrow-band

luminescence with long decay times and exceptionally long nuclear spin coherence times [18,19]. Therefore, one may expect that diamonds containing luminescence RE ions would find diverse applications in quantum computing, sensing, and biomedicine.

The realization of the challenging task of combining the extreme properties of diamonds with the exceptional optical and magnetic characteristics of rare-earth ions is at the very beginning. Magyar and co-workers were the first who demonstrated a method for fabricating diamonds containing luminescent europium-related defects [20]. This approach, based on the use of Eu-containing precursors and multistage chemical vapor deposition (CVD) diamond growth, was further developed in the recent work of Vanpoucke et al. [21]. The results of this combined theoretical/experimental study indicated possible incorporation of Eu defects in diamonds and shed light on important questions about the stability and electronic structure of various defect configurations involving RE ions [21]. Cajzl and co-workers reported successful fabrication of single- and nanocrystalline diamonds with luminescent Er defects using ion implantation techniques [22]. Fabrication of a diamond/rare-earth composite material with luminescent EuF_3 nanoparticles embedded in microcrystalline CVD diamond films was demonstrated by Sedov et al. [23]. At high-pressure, high-temperature (HPHT) conditions, synthesis of diamonds from "rare-earth element/carbon" binary systems was reported by Ekimov and co-workers [24]. They showed that Tm, Eu, and Er had a catalytic ability for converting graphite to diamond. The cathodoluminescence spectra of synthesized diamonds were dominated by fast-emitting nitrogen-vacancy centers (N3, H3, and NV^0) and showed no features because of the slowly emitting RE ions [24,25]. To the best of our knowledge, no other studies on HPHT synthesis and characterization of diamonds from systems containing rare-earth elements have been reported to date.

Recent investigations have demonstrated the significant potential of Mg-based solvent-catalysts for producing diamond crystals doped with impurity elements having covalent radii much greater than that of carbon [26,27]. It was found that that ultra-reduced Mg-based systems enable effective doping of diamonds with silicon [28], germanium [29], and tin [30] impurities with formation of optically active silicon-vacancy, germanium-vacancy, and tin-vacancy centers. Also, it is worth noting that Mg-based catalysts provide conditions for diamond crystallization in the kinetically controlled regime with very high growth rates, reaching 8.5 mm/h [27], and the produced diamond crystals are nitrogen-free type II. Although rare-earth ions have even larger covalent radii, it is reasonable to investigate diamond crystallization processes in the Mg-C system with the addition of rare-earth compounds and to perform spectroscopic characterization of synthesized diamonds. In the present study, we have chosen to use oxides of Nd, Sm, Eu, Gd, Tb, Dy, Ho, Er, Tm, and Yb as the RE-containing substances. Taking into account the specific features of diamond crystallization in Mg-based systems, their unusual growth mechanisms, crystal morphology, and properties, it is also of interest to assess the influence of rare-earth oxide additives on diamond crystallization processes and diamond crystal characteristics.

2. Materials and Methods

Diamond synthesis experiments were performed at a pressure of 7.8 GPa, a temperature of 1800 °C, and a run time of 30 min using a split-sphere, multi-anvil, high-pressure apparatus. Design of the high-pressure cell used in the experiments and details of the calibration of the P-T parameters have been presented in our previous works [27,31]. The starting materials were graphite rods (99.97% purity), metallic magnesium (99.99% purity), and oxides of rare-earth elements Nd_2O_3, Sm_2O_3, Eu_2O_3, Tb_2O_3, Dy_2O_3, Ho_2O_3, Er_2O_3, Tm_2O_3, and Yb_2O_3 (all purity 99.99%). A mixture of Mg and RE oxides together with four synthetic diamond seed crystals (~500 μm) were placed in thick-walled graphite capsules with a diameter of 6.9 mm, a height of 6.5 mm, and a wall thickness of 1.5 mm. The starting reagents and assembled high-pressure cells were dried at 120 °C for 15 h using a vacuum oven, which before opening was refilled with an inert gas (argon). In all experiments, graphite capsules were insulated from the outside with a Mo foil 0.1 mm thick that protected the capsules from interaction with high-pressure cell materials. After experiments, the samples were treated in a hot mixture of nitric

and hydrochloric acids (1:3 ratio by volume) to dissolve metals and carbides. Graphite was dissolved in a hot mixture of concentrated H_2SO_4 and 30% water solution of $K_2Cr_2O_7$ taken in 3:2 volume proportion. Residual graphite and the newly formed diamond were weighed to determine the degree of graphite-to-diamond conversion (α) in each experiment, which was defined as $\alpha = M_{Dm}/(M_{Dm} + M_{Gr}) \times 100$, where M_{Dm} is the mass of the synthesized diamond, and M_{Gr} is the mass of residual graphite. The recovered diamond crystals were studied using a Carl Zeiss Axio Imager Z2m optical microscope (Carl Zeiss Microscopy, Jena, Germany) and a Tescan MIRA3 LMU scanning electron microscope (Tescan, Brno, Czech Republic). Spectroscopic characterization of synthesized diamond crystals was performed by means of infrared (IR) absorption and photoluminescence (PL). IR spectra were recorded using a Bruker Vertex 70 Fourier-transform infrared (FTIR) spectrometer fitted with a Hyperion 2000 microscope (Bruker Optics, Ettlingen, Germany). PL spectra were measured using a custom-built setup based on a Horiba JY iHR320 monochromator equipped with a Syncerity CCD detector (Horiba Jobin Yvon S.A.S., Lonjumeau, France). Gratings with 2400, 1800, and 600 grooves/mm were selected from the turret depending on the desired spectral resolution and/or spectral range. Photoluminescence was excited using continuous-wave lasers operating at 395 nm (Omicron-Laserage Laserprodukte GmbH, Rodgau-Dudenhofen, Germany), 473 nm and 532 nm (Laser Quantum, Stockport, UK). An achromatic lens with a focal length of 60 mm was used to focus the laser beam (to a spot of ~20 μm in diameter) onto the sample and to collect the photoluminescence signal. Proper optical long-pass edge filters were placed between the collecting lens and a lens (f = 120 mm) that focused the PL emission onto an entrance slit of the monochromator. A Linkam FTIR600 heating/freezing stage (Linkam Scientific Instruments, Tadworth, UK) mounted on an XYZ translation stage was used for the low-temperature measurements. The optical scheme also involved an additional switchable channel equipped with a digital camera allowing visualization and control of the laser spot position over the sample.

3. Results and Discussion

3.1. Diamond Crystallization

The experimental parameters, starting compositions, and main results of experiments on diamond synthesis the Mg-R_2O_3-C systems (where R = Nd, Sm, Eu, Gd, Tb, Dy, Ho, Er, Tm, and Yb) are presented in Table 1. In experiments R1-R10, the content of R_2O_3 was 10 wt %, and the pressure (7.8 GPa), temperature (1800 °C), and duration (30 min) were chosen to ensure synthesis of relatively large crystals suitable for characterization by different spectroscopic techniques. In the control experiment (M-1) performed in the Mg-C system with the same synthesis parameters, diamond crystals with cubic morphology were produced, with the degree of the graphite-to-diamond conversion (α) being approximately 80%. When 10 wt % R_2O_3 was added to the system, the degree of the graphite-to-diamond conversion almost did not change and was estimated at a level of 70%–90%, indicating a slight effect of 10 wt % of rare-earth oxide additives on diamond crystallization processes.

Spontaneous nucleation of diamond occurred at the interface between the catalyst melt and the graphite capsule. The crystals then grew predominantly in the direction of graphite, and as a result, an aggregate of diamond crystals with various sizes was formed. After dissolving the catalyst, the aggregate disintegrated into separate crystals and blocks.

The recovered diamond crystals formed intergrowths and twins with sizes up to 2.0 mm. Crystals grown on the seeds reached 2.7 mm in size. The morphology of diamonds synthesized in runs R1-R10 was determined by {100} faces. Sometimes, weakly developed {111} faces were also present. The color of the synthesized diamond crystals varied from colorless to brown. Some crystals were black. Transparent crystals frequently exhibited zoning along the {100} direction, which appeared as an alternation of zones of different colors (Figure 1a).

Table 1. Experimental conditions and results.

Run No.	Composition, wt %	P, GPa	T, °C	Time, min	Diamond Growth on Seed	Diamond Nucleation	α, %	Metastable Graphite
M-1	Mg	7.8	1800	30	+	+	80	-
R-1	Mg + d_2O_3 10%	7.8	1800	30	+	+	90	-
R-2	Mg + Sm_2O_3 10%	7.8	1800	30	+	+	80	-
R-3	Mg + Eu_2O_3 10%	7.8	1800	30	+	+	70	-
R-4	Mg + Gd_2O_3 10%	7.8	1800	30	+	+	75	-
R-5	Mg + Tb_2O_3 10%	7.8	1800	30	+	+	75	-
R-6	Mg + Dy_2O_3 10%	7.8	1800	30	+	+	70	-
R-7	Mg + Ho_2O_3 10%	7.8	1800	30	+	+	80	-
R-8	Mg + Er_2O_3 10%	7.8	1800	30	+	+	85	-
R-9	Mg + Tm_2O_3 10%	7.8	1800	30	+	+	75	-
R-10	Mg + Yb_2O_3 10%	7.8	1800	30	+	+	80	-
R-11	Mg + Sm_2O_3 20%	7.8	1800	30	+	+	40	-
R-12	Mg + Sm_2O_3 30%	7.8	1800	30	+	+	10	-
R-13	Mg + Sm_2O_3 40%	7.8	1800	30	+	-	0	+
R-14	Mg + Sm_2O_3 50%	7.8	1800	30	-	-	0	+

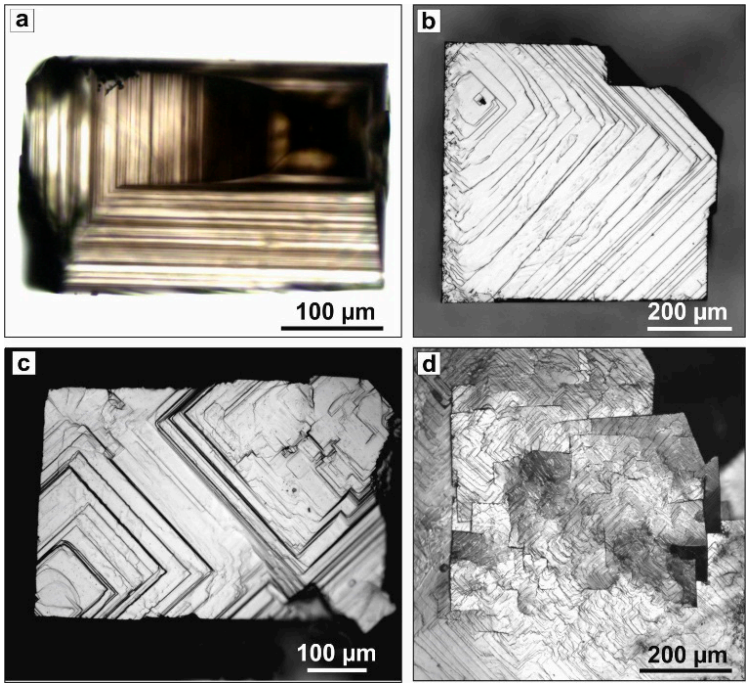

Figure 1. Optical micrographs of surface microrelief and internal structure of diamond crystals produced in the Mg-R_2O_3-C systems: (**a**) zoning along the {100} face (transmitted light, run R-3); (**b**) stepped {100} face with a single growth center (run R-3); (**c**) clusters of macrosteps trains from several growth centers (run R-9); and (**d**) block structure of the {100} face (run R-6).

The microrelief of the {100} face had different specific features depending on the intensity of sample coloration. Transparent, nearly colorless crystals had smooth {100} faces, which typically showed echelons of growth steps of different heights extending in the {110} directions (Figure 1b). The steps extended from single point sources, which were either microtwin insets or places of intergrowth of different crystals. The ends of the growth layers were often not straight. The presence of numerous kinks on the steps led to the deviation of their shape from the correct rectangular shape.

Dark-colored, transparent diamonds had a more rugged relief (Figure 1c). Clusters of steps formed echelons of macrosteps, which often spread from several sources. The {100} faces of black opaque diamond crystals had the coarsest relief (Figure 1d). They were characterized by a mosaic

structure because of the presence of disoriented blocks. The growth steps, extending from the borders of numerous blocks, formed a complex, highly rugged relief on the {100} faces.

In the second series of experiments, we studied the effect of higher contents of rare-earth oxides on diamond crystallization in the Mg-R_2O_3-C system. For this study, samarium oxide (Sm_2O_3) was chosen as the additive. The choice of Sm_2O_3, as it will be shown below, was partly substantiated by the observation of some photoluminescence features deserving more detailed examination. In this series of experiments, the amount of Sm_2O_3 additive was changed from 0 to 50 wt %, while the experimental procedures and the P-T-t parameters were constant.

With the addition of 10 wt % Sm_2O_3 (R-2), the degree of graphite-to-diamond conversion was 80%. The diamond formed crystals, intergrowths, and twins with color ranging from nearly colorless to brown and black. The maximum size of the crystals synthesized in the R-2 experiment was 1.65 mm; consequently, the maximum growth rate was 1.65 mm/h. At 20 wt % Sm_2O_3 (R-11), the produced crystals had similar morphologies and colors as those from run R-2; however, in this case, the size of the crystals did not exceed 1 mm, and the degree of conversion of graphite to diamond was 40%. With 30 wt % Sm_2O_3 additive (run R-12), the size of the synthesized diamonds did not exceed 300 μm, indicating a further decrease in the growth rate down to 0.3 mm/h. The produced crystals showed diverse morphologies. Crystals with cubic habits, which demonstrated pronounced growth macrolayers, and their intergrowths were found (Figure 2a). Some crystals had a cuboctahedral habit with stepped surfaces on the {100} and {111} faces. The faces were composed of rectangular and triangular macrolayers whose areas decreased to the face center. As a result, the faces attained a typical antiskeletal structure, and the edges of the growth layers formed trapezohedron pseudofaces (Figure 2b). Sometimes crystals acquired a rounded shape because of the convex and block {100} and {111} faces (Figure 2c). The observed diversity of crystal morphologies from cube to cuboctahedron, in our opinion, was related to changes in the solvent-catalyst properties and its possible heterogeneity. Decreasing diamond growth rate, increasing relative development of the {111} faces, and formation of antiskeletal crystals have been previously observed in a number of studies on diamond crystallization from Mg-based catalysts with different additives [28,29,32,33]. It was clear that increasing the Sm_2O_3 content to 30 wt % led to a change in the diamond growth mechanism caused by enhanced blocking of the growth step propagation by the adsorbed impurities. These impurities can be related to oxygen-containing complexes adsorbed on the diamond surface. The adverse influence of excess oxygen on diamond crystal growth has been established previously for the $Ni_{0.7}Fe_{0.3}$-C system [34] and systems based on the Mg catalyst [32].

An increase in the Sm_2O_3 content of the growth system to 40% (R-13) led to complete termination of spontaneous nucleation of diamond and the formation of a large amount of metastable graphite in the crystallization capsule. Diamond seed crystals partially dissolved by about 30%–40%, and then they regenerated with the formation of {100} and {111} growth faces and {110} stepped surfaces formed by {100}, {111}, and trapezohedron faces (Figure 2d). At 50 wt % Sm_2O_3 (run R-14), no diamond growth was detected, and only newly formed crystals of metastable graphite were found in the run products. The seed crystals dissolved by approximately 50%.

Figure 3 shows the degree of graphite-to-diamond conversion (α) as a function of the Sm_2O_3 content in the system. It clearly demonstrated an inhibitory effect of the oxide on diamond crystallization processes. It should be noted that in all experiments with Sm_2O_3 additives, no newly formed phases, except diamond or graphite, were established. It was most likely that diamond crystallized from the Mg-Sm-O-C melt, and with an increase in the Sm_2O_3 content, the composition of the melt changed corresponding to the starting composition of the system. The morphology of diamond crystals synthesized at 30 wt % Sm_2O_3 (R-12) was characterized by elements of antiskeletal growth, which were produced in growth inhibition processes [32,34]. The observed changes in the degree of graphite-to-diamond conversion, the changeover of diamond crystallization to the crystallization of metastable graphite, and the changes in the diamond crystal morphology with increasing the Sm_2O_3 content attested the inhibiting effect of the oxide on diamond crystallization processes in the Mg-Sm-O-C system.

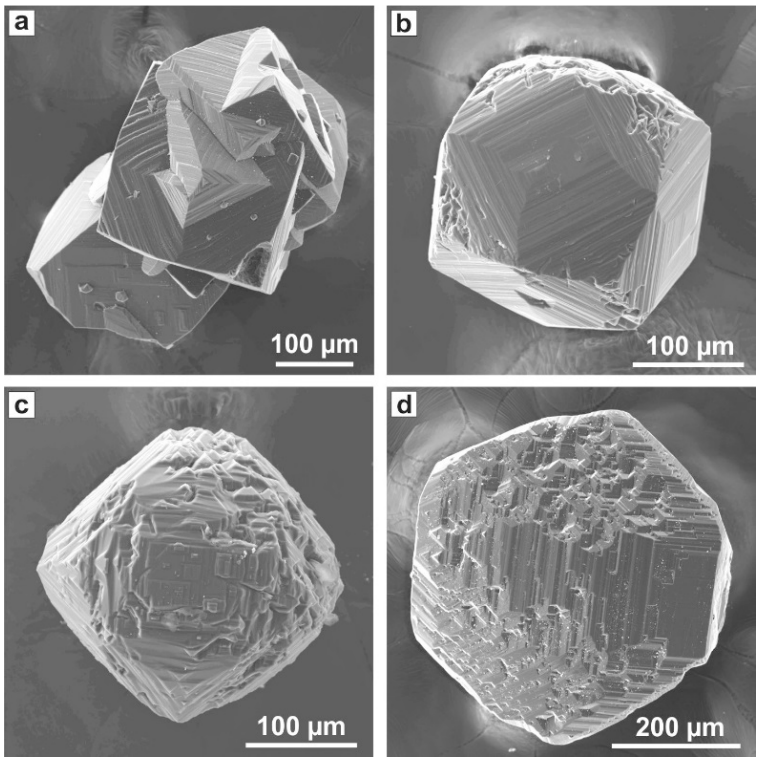

Figure 2. SEM micrographs of diamond crystals produced in the Mg-Sm_2O_3-C system: (**a**) intergrowth of twins and crystals of the diamond (run R-12); (**b**) a cuboctahedral diamond crystal with stepped trapezohedron faces (run R-12); (**c**) a rounded crystal bound by curve-faced surfaces (run R-12); and (**d**) regenerated surface of the seed crystal (run R-13).

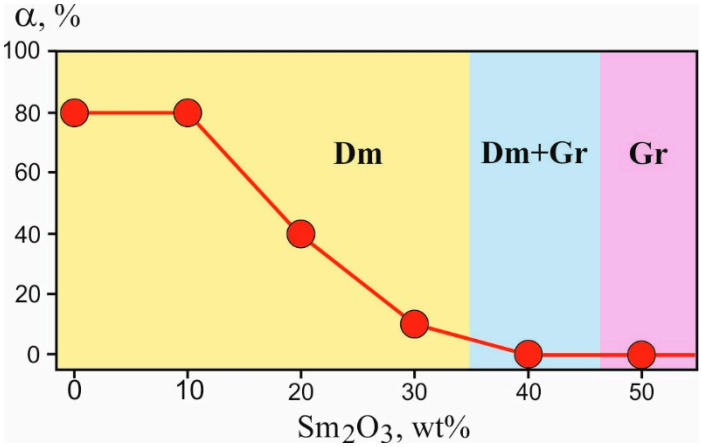

Figure 3. Degree of graphite-to-diamond conversion (α, %) in the Mg-Sm_2O_3-C system as functions of Sm_2O_3 concentration (wt %). For further explanations, see the text.

3.2. Spectroscopic Characterization

Diamond crystals synthesized in the Mg-R_2O_3-C system were studied by means of infrared absorption and photoluminescence techniques. We began by considering the results obtained for the first series of experiments performed with the addition of a fixed amount (10 wt %) of different rare-earth oxides to the Mg catalyst. For infrared measurements, diamond samples representing typical products were selected from each synthesis run. When possible, the samples were mechanically polished from two sides to provide optical windows. Infrared absorption measurements did not reveal significant differences in the spectra of diamonds synthesized with different starting compositions.

It was found that nearly colorless diamond crystals or crystal areas in the IR spectra showed either no impurity-related absorption, corresponding to type IIa diamond, or relatively weak absorption features related to boron impurities (type IIb) (Figure 4). The concentration of the uncompensated boron acceptors in the studied samples was estimated to be less than 0.5 ppm. The spectra recorded for brown-colored crystals or crystal areas, in addition to the absorption due to the boron acceptors, showed an absorption that steadily increased toward larger wavenumbers (Figure 4). Similar absorption spectra were previously found to be typical for brown-colored diamonds produced in the Mg-C system, and the continuous absorption was suggested to originate from defects involving π-bonded carbon atoms (e.g., vacancy clusters [26,27]). For diamond crystals that were black and opaque, it was not possible to acquire IR absorption spectra.

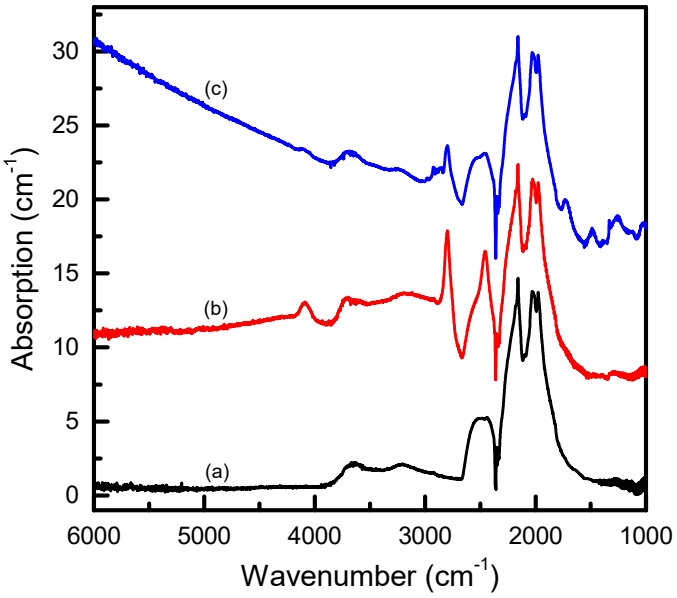

Figure 4. Typical infrared absorption spectra of diamond crystals synthesized in the Mg-10wt%R_2O_3-C system. The spectra were measured for (**a, b**) nearly colorless and (**c**) brown crystals from run R-2. The spectra are displaced vertically for clarity.

Photoluminescence measurements were performed for both the diamond samples used in the infrared measurements and a number of additional smaller samples (100–200 μm) selected from each run. It was found that, irrespective of the growth system composition, the dominant feature present in the PL spectra in the overwhelming majority of the samples was a vibronic band with a zero-phonon line at 737 nm caused by the negatively charged silicon-vacancy centers (Si-V$^-$) (Figure 5). It should be noted that the main source of silicon impurities in the growth system was the starting graphite that contained approximately 120 wt ppm Si [35]. As a rule, the relative PL intensity of the SiV$^-$ centers (normalized to the intensity of the first-order diamond Raman peak) was higher for the crystals or crystal areas showing brown coloration. In the PL spectra of crystals that appeared black and opaque, the SiV$^-$ centers were also present as the major luminescence feature, but they showed a significantly broader zero-phonon line (ZPL), suggesting a high level of internal strain in these crystals. Colorless crystals or crystal zones in addition to the SiV$^-$ centers frequently exhibited PL bands because of the nitrogen-vacancy centers. PL spectra recorded with different excitation lasers (wavelengths 395, 473, and 532 nm) revealed neutral and negatively charged N-V centers with zero-phonon lines at 575 and 637 nm, respectively, H3 centers with ZPLs at 503 nm, and N3 centers with ZPLs at 415 nm (Figure 5). In addition, we noted the occurrence of a peak at 720 nm, which frequently accompanied the 737 nm peak of the SiV$^-$ centers but had much weaker intensity. In general, the results obtained for this series of synthesis experiments broadly agreed with the previous works on studying diamonds crystallized from Mg-based solvent-catalysts [26,27]. These results

suggested that the addition of 10 wt % R_2O_3 did not significantly affect the spectroscopic characteristics of the crystallized diamond as compared to those produced in the undoped Mg-C system.

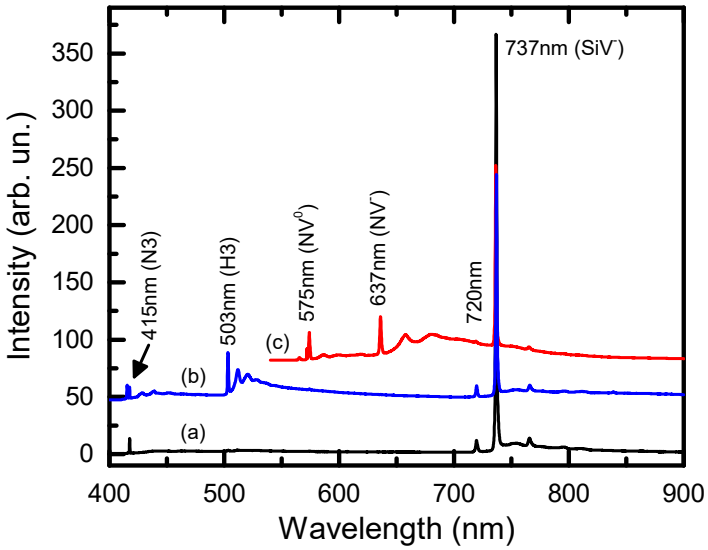

Figure 5. Representative photoluminescence spectra of diamond crystals synthesized in the Mg-10wt%R_2O_3-C system. The spectra were measured for diamond samples from run R-1 with the excitation with a 395 nm laser (spectra (**a**) and (**b**)) and a 532 nm laser (spectrum (**c**)). The spectra are displaced vertically for clarity.

It is necessary to emphasize that no luminescence features resembling the emission spectra of the rare-earth ions were detected for diamonds synthesized with all rare-earth oxide additives used in this study, with the exception of Sm_2O_3. In the latter case, we noted that diamond crystals synthesized with the addition of 10 wt % Sm_2O_3 frequently exhibited in PL spectra a group of weak emission lines located between 650–670 nm (Figure 6). The observation of these peaks, which could possibly be related to samarium ions, prompted us to choose samarium oxide for the study of the effect of higher contents of rare-earth oxides on diamond crystallization in the Mg-R_2O_3-C system. As it was described in the preceding section, diamond crystals produced with the addition of 20 wt % Sm_2O_3 (run R-11) were overall similar to those synthesized with 10 wt % Sm_2O_3, with the main difference being somewhat lower crystal sizes. Figure 6 shows a typical PL spectrum recorded for diamond crystals from run R-11 with 395 nm laser excitation. The remarkable characteristic of the spectrum was the occurrence of relatively intense emission lines comprising four groups centered at approximately 580, 620, 670, and 725 nm. Each group consisted of a number of closely spaced narrow peaks with different intensities. Note that the lines grouped at around 670 nm having the highest relative intensity were essentially the same as those observed for diamond crystals synthesized with 10 wt % Sm_2O_3 additive.

Considering the possible nature of the observed luminescence spectrum, which is shown in Figure 7 in greater detail, we noted that it resembled to some extent the emission spectrum characteristic of Sm^{3+} ions. For comparison, Figure 7 also demonstrates a PL spectrum recorded for Sm_2O_3 powder used in this study as the starting reagent. The emission spectrum of trivalent samarium ions in the visible range typically consisted of four bands corresponding to the 4f-4f electronic transitions from the $^4G_{5/2}$ level to the different ^6H_J manifolds (where J = 5/2, 7/2, 9/2, and 11/2), which were typically located at approximately 560, 600, 650, and 700 nm [36,37]. The spectral position of the bands, their relative intensities, and multiplet splitting were influenced by the local symmetry of the Sm^{3+} ion and the nature of the ligands [38,39]. The low-symmetry environments caused the emission bands to split into Stark components (up to J + 1/2 sublevels) and led to the higher relative intensity of the hypersensitive $^4G_{5/2} \rightarrow {}^6H_{9/2}$ transition ($\lambda \sim 650$ nm) [39,40]. The frequencies of the 4f-4f transitions can be affected by the nature of the chemical bonding through the so-called "nephelauxetic effect", which is attributed to a covalent contribution to the bonding between the lanthanide ions

and the ligands [40,41]. As a rule, with an increasing covalency degree, the 4f-4f emission band maxima shifted to longer wavelengths (red shift) [40,41]. With these premises in mind, we hypothesized that the specific luminescence spectrum observed in this work was associated with Sm^{3+} ions, which should (1) be located on low-symmetry lattice sites and (2) have a high degree of covalent bonding character with the host atoms. The most intriguing question then was: What was the nature of these Sm-containing species? Namely, could they be Sm-related lattice defects formed in the diamond crystal structure, or could they represent some Sm-containing compounds entrapped by the growing diamond crystals as microinclusions?

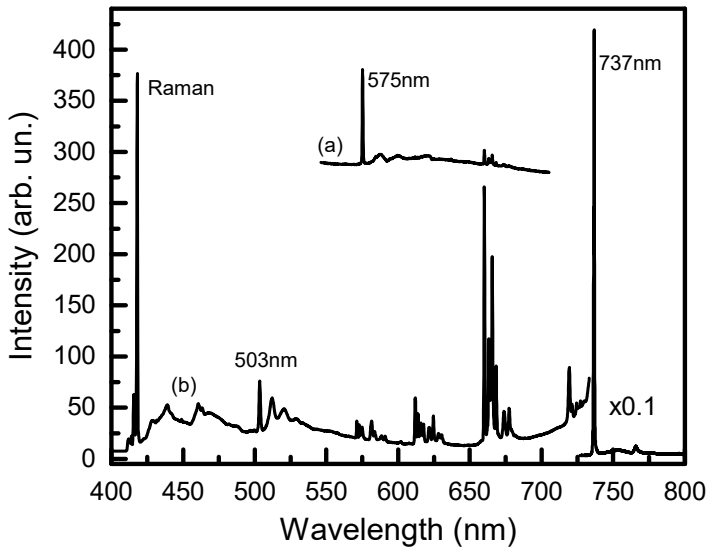

Figure 6. Photoluminescence (PL) spectra of diamond crystals synthesized with (**a**) 10 wt % and (**b**) 20 wt % of Sm_2O_3 additives. PL was excited with a 395 nm laser. Spectrum (**a**) is arbitrarily scaled to facilitate comparison. The near-infrared part of spectrum (**b**) is multiplied by a factor of 0.1. The spectra are displaced vertically for clarity.

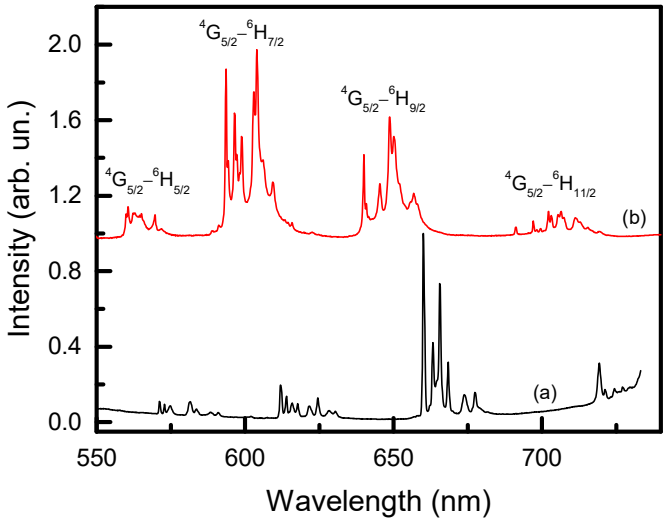

Figure 7. Photoluminescence spectra of (**a**) diamond crystals synthesized with 20 wt % of Sm_2O_3 additives (λ_{exc} = 395 nm), and (**b**) Sm_2O_3 powder (λ_{exc} = 473 nm). The spectra are normalized to the maximum intensity and displaced vertically for clarity.

Let us now consider the results obtained from the PL measurements on diamond crystals synthesized with 30 wt % Sm_2O_3 additive. As it was described in the preceding section, diamond crystals produced in this case showed a number of significant differences as compared to those

synthesized with lower amounts of Sm_2O_3 additives. These included considerably smaller crystal sizes, which did not exceed 300 μm, implying growth rates approximately 5.5 times lower than in the run R-2 with 10 wt % Sm_2O_3, and the abundance of crystals with diverse morphologies. For the PL measurements, samples representing typical products were selected. The obtained spectra were qualitatively similar for all the samples examined, and a typical one is shown in Figure 8. Several main observations were made from the analysis of the measured spectra. First, the nitrogen-vacancy centers (N3, H3, NV^0, NV^-) appeared more abundant in photoluminescence. Second, the PL from the SiV^- centers decreased in relative intensity. Third, no specific photoluminescence signal, which was found for diamonds synthesized with lower amounts of Sm_2O_3 additives and tentatively assigned to Sm^{3+} ions, was detected in the spectra. It was likely that the addition of 30 wt % Sm_2O_3 was sufficient to change the properties of the solvent-catalyst resulting in a higher uptake of nitrogen impurities and less effective formation of silicon-vacancy centers. The absence of the peculiar PL spectrum observed for diamonds synthesized with lower Sm_2O_3 contents was not very clear, but this seemed to indicate that the Sm-related defect nature of this PL signal was favored rather than inclusions of an Sm-containing compound. To resolve this question, further investigations involving micro-Raman/PL measurements are necessary and currently underway.

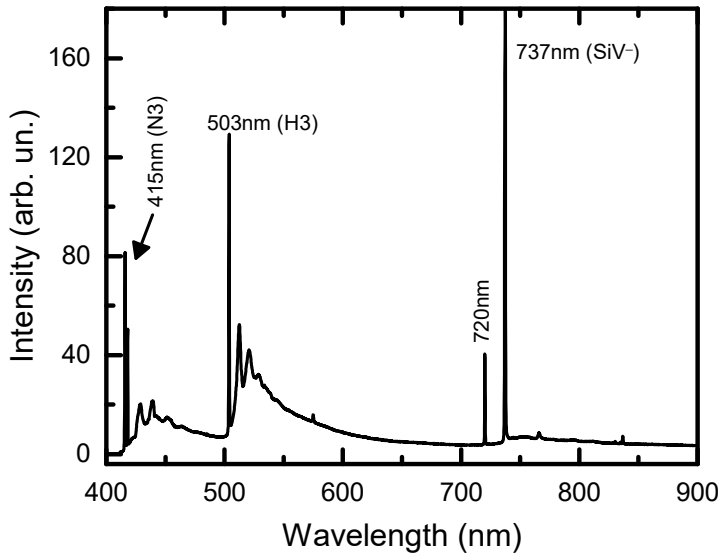

Figure 8. Typical PL spectrum of diamond crystals synthesized with 30 wt % of Sm_2O_3 additives. PL was excited with a 395 nm laser.

We finish this section by commenting on the fact that only diamonds synthesized with the samarium oxide additive showed a specific photoluminescence signal, suggesting possible involvement of a rare-earth ion. First, it was noted that for some of the RE elements used in this work, characteristic emission spectra were in the near-infrared range where the sensitivity of the employed PL setup was low. Second, it was known that the RE ions had narrow-band PL excitation spectra, so the laser wavelengths we were able to use could not fit the corresponding excitation bands. Also, we did not exclude that there were some chemical reasons that influenced incorporation of the rare-earth elements. In this respect, it will be interesting to examine diamond crystals synthesized in this work using time-resolved cathodoluminesce spectroscopy, which would enable filtering out the luminescence of the slow-emitting rare-earth ions (typical decay times ~0.1–1 ms) from that of the fast-emitting nitrogen-vacancy centers (typical decay times ~1–10 ns).

4. Summary

Diamond crystallization in Mg-R_2O_3-C systems (R = Nd, Sm, Eu, Tb, Dy, Ho, Er, Tm, and Yb) was studied at 7.8 GPa and 1800 °C. It was found that the rare-earth oxide additives in an amount of 10 wt %

did not significantly affect the degree of graphite-to-diamond conversion (α = 70%–90%) relative to the Mg-C system (α = 80%). The morphology of diamonds synthesized in the Mg-$R_2O_3$10 wt % systems was mainly determined by the {100} faces. The surface microreliefs of the {100} faces were associated with crystal defectiveness and had specific features depending on the color of the crystals (colorless, brown, or black).

The effect of higher amounts of RE oxide additives on diamond crystallization has been studied for the Mg-Sm_2O_3-C system with a Sm_2O_3 content varied from 0 to 50 wt %. It was established that with an increase in the Sm_2O_3 content in the growth system, the degree of graphite-to-diamond conversion decreased from 80% at 10% Sm_2O_3 to 0% at 40% Sm_2O_3. At high Sm_2O_3 contents (40 and 50 wt %), instead of diamond, mass crystallization of metastable graphite was established. An increase in the concentration of Sm_2O_3 in the growth system led to a change in diamond morphology from a cube to a polyhedron, formed by the trapezohedral, cubic, and octahedral faces, as well as a significant decrease in the diamond growth rate from 1.65 to 0.3 mm/h. The established regularities unambiguously indicated the inhibiting role of oxide on diamond crystallization processes in the Mg-Sm-O-C system.

The crystallized diamonds were studied by a suite of optical spectroscopy techniques, and the major characteristics of their defect-and-impurity structure were revealed. It was found that the addition of rare-earth oxides in the amount of 10 wt % did not significantly affect the spectroscopic characteristics of the synthesized diamonds as compared to those produced in the undoped Mg-C system. For diamond crystals produced with 10 wt % and 20 wt % Sm_2O_3, a specific photoluminescence signal comprising four groups of lines centered at approximately 580, 620, 670, and 725 nm was detected. This PL spectrum can be tentatively assigned to the emission characteristic of Sm^{3+} ions. Establishing the nature of the luminescent Sm^{3+} species requires further investigations.

Author Contributions: conceptualization, Y.N.P.; methodology, Y.N.P. and Y.M.B.; investigation, Y.N.P., Y.M.B., A.F.K., and I.N.K.; writing—original draft preparation, Y.N.P., A.F.K., and I.N.K.; writing—review & editing, Y.N.P., I.N.K.

Funding: This research was funded by the Russian Foundation for Basic Research, grant number 18-29-12041, and the Ministry of Science and Higher Education of the Russian Foundation, state assignment project IGM SB RAS.

Acknowledgments: The authors thank Denis Nechaev and Tatyana Molyavina for their technical support in the course of the study.

Conflicts of Interest: The authors declare no conflict of interest. The funders had no role in the design of the study; in the collection, analyses, or interpretation of data; in the writing of the manuscript, or in the decision to publish the results.

References

1. Takeuchi, S. Recent progress in single-photon and entangled-photon generation and applications. *Jpn. J. Appl. Phys.* **2014**, *53*, 030101. [CrossRef]
2. Orwa, J.O.; Greentree, A.D.; Aharonovich, I.; Alves, A.D.C.; Van Donkelaar, J.; Stacey, A.; Prawer, S. Fabrication of single optical centres in diamond - A review. *J. Lumin.* **2010**, *130*, 1646–1654. [CrossRef]
3. Schloss, J.M.; Barry, J.F.; Turner, M.J.; Walsworth, R.L. Simultaneous broadband vector magnetometry using solid-state spins. *Phys. Rev. Appl.* **2018**, *10*, 034044. [CrossRef]
4. Casola, F.; van der Sar, T.; Yacoby, A. Probing condensed matter physics with magnetometry based on nitrogen-vacancy centres in diamond. *Nat. Rev. Mater.* **2018**, *3*, 17088. [CrossRef]
5. Barnard, A.S. Diamond standard in diagnostics: nanodiamond biolabels make their mark. *Analyst* **2009**, *134*, 1751–1764. [CrossRef]
6. Mohan, N.; Chen, C.S.; Hsieh, H.H.; Wu, Y.C.; Chang, H.C. In vivo imaging and toxicity assessments of fluorescent nanodiamonds in caenorhabditis elegans. *Nano Lett.* **2010**, *10*, 3692–3699. [CrossRef] [PubMed]
7. Chu, Y.; Lukin, M.D. Quantum optics with nitrogen-vacancy centres in diamond. In *Quantum Optics and Nanophotonics*; Fabre, C., Sandoghdar, V., Treps, N., Cugliandolo, L.F., Eds.; Oxford University: Oxford, UK, 2017; pp. 229–270.

8. Wrachtrup, J.; Jelezko, F. Processing quantum information in diamond. *J. Phys. Condens. Matter.* **2006**, *18*, S807–S824. [CrossRef]
9. Neumann, P.; Kolesov, R.; Naydenov, B.; Beck, J.; Rempp, F.; Steiner, M.; Jacques, V.; Balasubramanian, G.; Markham, M.L.; Twitchen, D.J.; et al. Quantum register based on coupled electron spins in a room-temperature solid. *Nat. Phys.* **2010**, *6*, 249–253. [CrossRef]
10. Sipahigil, A.; Jahnke, K.D.; Rogers, L.J.; Teraji, T.; Isoya, J.; Zibrov, A.S.; Jelezko, F.; Lukin, M.D. Indistinguishable photons from separated silicon-vacancy centers in diamond. *Phys. Rev. Lett.* **2014**, *113*, 113602. [CrossRef]
11. Sukachev, D.D.; Sipahigil, A.; Nguyen, C.T.; Bhaskar, M.K.; Evans, R.E.; Jelezko, F.; Lukin, M.D. Silicon-vacancy spin qubit in diamond: a quantum memory exceeding 10 ms with single-shot state readout. *Phys. Rev. Lett.* **2017**, *119*, 223602. [CrossRef]
12. Siyushev, P.; Metsch, M.H.; Ijaz, A.; Binder, J.M.; Bhaskar, M.K.; Sukachev, D.D.; Sipahigil, A.; Evans, R.E.; Nguyen, C.T.; Lukin, M.D.; et al. Optical and microwave control of germanium-vacancy center spins in diamond. *Phys. Rev. B.* **2017**, *96*, 081201(R). [CrossRef]
13. Bhaskar, M.K.; Sukachev, D.D.; Sipahigil, A.; Evans, R.E.; Burek, M.J.; Nguyen, C.T.; Rogers, L.J.; Siyushev, P.; Metsch, M.H.; Park, H.; et al. Quantum nonlinear optics with a germanium-vacancy color center in a nanoscale diamond waveguide. *Phys. Rev. Lett.* **2017**, *118*, 223603. [CrossRef] [PubMed]
14. Iwasaki, T.; Miyamoto, Y.; Taniguchi, T.; Siyushev, P.; Metsch, M.H.; Jelezko, F.; Hatano, M. Tin-vacancy quantum emitters in diamond. *Phys. Rev. Lett.* **2017**, *119*, 253601. [CrossRef] [PubMed]
15. Tchernij, S.D.; Herzig, T.; Forneris, J.; Kupper, J.; Pezzagna, S.; Traina, P.; Moreva, E.; Degiovanni, I.P.; Brida, G.; Skukan, N.; et al. Single-photon-emitting optical centers in diamond fabricated upon Sn implantation. *ACS Photonics* **2017**, *4*, 2580. [CrossRef]
16. Trusheim, M.E.; Wan, N.H.; Chen, K.C.; Ciccarino, C.J.; Flick, J.; Sundararaman, R.; Malladi, G.; Bersin, E.; Walsh, M.; Lienhard, B.; et al. Lead-related quantum emitters in diamond. *Phys. Rev. B.* **2019**, *99*, 075430. [CrossRef]
17. Tchernij, S.D.; Lühmann, T.; Forneris, J.; Herzig, T.; Küpper, J.; Damin, A.; Santonocito, S.; Traina, P.; Moreva, E.; Celegato, F.; et al. Photoluminescence of lead-related optical centers in single-crystal diamond. *ACS Photonics* **2018**, *5*, 4864–4871.
18. Kenyon, A.J. Recent developments in rare-earth doped materials for optoelectronics. *Prog. Quantum Electron.* **2002**, *26*, 225–284. [CrossRef]
19. Zhong, M.; Hedges, M.P.; Ahlefeldt, R.L.; Bartholomew, J.G.; Beavan, S.E.; Wittig, S.M.; Longdell, J.J.; Sellarset, M.J. Optically addressable nuclear spins in a solid with a six-hour coherence time. *Nature* **2015**, *517*, 177–180. [CrossRef]
20. Magyar, A.; Hu, W.; Shanley, T.; Flatte, M.E.; Hu, E.; Aharonovich, I. Synthesis of luminescent europium defects in diamond. *Nat. Commun.* **2014**, *5*, 3523. [CrossRef]
21. Vanpoucke, D.E.P.; Nicley, S.S.; Raymakers, J.; Maes, W.; Haenen, K. Can europium atoms form luminescent centres in diamond: A combined theoretical–experimental study. *Diamond Relat. Mater.* **2019**, *94*, 233–241. [CrossRef]
22. Cajzl, J.; Akhetova, B.; Nekvindova, P.; Mackova, A.; Malinsky, P.; Oswald, J.; Remes, Z.; Varga, M.; Kromka, A. Co-implantation of Er and Yb ions into single-crystalline and nanocrystalline diamond. *Surf. Interface Anal.* **2018**, *50*, 1218–1223. [CrossRef]
23. Sedov, V.S.; Kuznetsov, S.V.; Ralchenko, V.G.; Mayakova, M.N.; Krivobok, V.S.; Savin, S.S.; Zhuravlev, K.P.; Martyanov, A.K.; Romanishkin, I.D.; Khomich, A.A.; et al. Diamond-EuF_3 nanocomposites with bright orange photoluminescence. *Diamond Relat. Mater.* **2017**, *72*, 47–52. [CrossRef]
24. Ekimov, E.A.; Zibrov, I.P.; Malykhin, S.A.; Khmelnitskiy, R.A.; Vlasov, I.I. Synthesis of diamond in double carbon-rare earth element systems. *Mater. Lett.* **2017**, *193*, 130–132. [CrossRef]
25. Ekimov, E.A.; Zibrov, I.P.; Malykhin, S.A.; Khmelnitskiy, R.A.; Vlasov, I.I. Luminescence properties of diamond prepared in the presence of rare-earth elements. *Inorg. Mater.* **2017**, *53*, 809–815. [CrossRef]
26. Palyanov, Y.N.; Borzdov, Y.M.; Kupriyanov, I.N.; Khokhryakov, A.F.; Nechaev, D.V. Diamond crystallization from an Mg-C system at high pressure high temperature conditions. *CrystEngComm* **2015**, *17*, 4928–4936. [CrossRef]
27. Palyanov, Y.N.; Kupriyanov, I.N.; Khokhryakov, A.F.; Borzdov, Y.M. High-pressure crystallization and properties of diamond from magnesium-based catalysts. *CrystEngComm* **2017**, *19*, 4459–4475. [CrossRef]

28. Palyanov, Y.; Kupriyanov, I.; Borzdov, Y.; Nechaev, D.; Bataleva, Y. HPHT Diamond Crystallization in the Mg-Si-C System: Effect of Mg/Si Composition. *Crystals* **2017**, *7*, 119. [CrossRef]
29. Palyanov, Y.N.; Kupriyanov, I.N.; Borzdov, Y.M.; Khokhryakov, A.F.; Surovtsev, N.V. High-pressure synthesis and characterization of Ge-doped single crystal diamond. *Cryst. Growth Des.* **2016**, *16*, 3510–3518. [CrossRef]
30. Palyanov, Y.N.; Kupriyanov, I.N.; Borzdov, Y.M. High-pressure synthesis and characterization of Sn-doped single crystal diamond. *Carbon* **2019**, *143*, 769–775. [CrossRef]
31. Sokol, A.G.; Borzdov, Y.M.; Palyanov, Y.N.; Khokhryakov, A.F. High temperature calibration a multi-anvil high-pressure apparatus. *High. Pres. Res.* **2015**, *35*, 139–147. [CrossRef]
32. Khokhryakov, A.F.; Sokol, A.G.; Borzdov, Y.M.; Palyanov, Y.N. Morphology of diamond crystals grown in magnesium-based systems at high temperatures and high pressures. *J. Cryst. Growth* **2015**, *426*, 276–282. [CrossRef]
33. Khokhryakov, A.F.; Palyanov, Y.N.; Borzdov, Y.M.; Kozhukhov, A.S.; Sheglov, D.S. Influence of a silicon impurity on growth of diamond crystals in Mg-C systems. *Diamond Relat. Mater.* **2018**, *87*, 27–34. [CrossRef]
34. Palyanov, Y.N.; Borzdov, Y.M.; Kupriyanov, I.N.; Khokhryakov, A.F. Effect of H_2O on diamond crystal growth in metal-carbon systems. *Cryst. Growth Des.* **2012**, *12*, 5571–5578. [CrossRef]
35. Palyanov, Y.N.; Kupriyanov, I.N.; Borzdov, Y.M.; Nechaev, D.V. Effect of the solvent-catalyst composition on diamond crystallization in the Mg-Ge-C system. *Diamond Relat. Mater.* **2018**, *89*, 1–9. [CrossRef]
36. Shionoya, S.; Yen, W.; Yamamoto, H. *Phosphor Handbook*, 2nd ed.; CRC Press: Boca Raton, FL, USA, 1999.
37. Baur, F.; Katelnikovas, A.; Sakirzanovas, S.; Petry, R.; Jüstel, T. Synthesis and optical properties of $Li_3Ba_2La_3(MoO_4)_8$:Sm^{3+} powders for pcLEDs. *Z. Naturforsch.* **2014**, *69b*, 183–192. [CrossRef]
38. Jorgensen, C.K.; Reisfeld, R. Chemistry and spectroscopy of lanthanides. *Top. Curr. Chem.* **1982**, *100*, 126–166.
39. Fan, X.; Freslon, S.; Daiguebonne, C.; Calvez, G.; Le Polles, L.; Bernot, K.; Guillou, O. Heteronuclear lanthanide-based coordination polymers exhibiting tunable multiple emission spectra. *J. Mater. Chem. C* **2014**, *2*, 5510–5525. [CrossRef]
40. Jorgensen, C.K. *Modern Aspects of Ligand Field Theory*, 1st ed.; North-Holland Pub. Co.: Amsterdam, The Netherlands, 1971; 538p.
41. Reisfeld, R. Optical properties of rare earths in condensed phase, theory and applications. *AIMS Mater. Sci.* **2015**, *2*, 37–60. [CrossRef]